MOMENTUM BALANCE FROM A HINDCAST AND NOWCAST MODEL OF CURRENTS IN THE SANTA BARBARA CHANNEL

Lie-Yauw Oey[1], Dong-Ping Wang[2], Clinton Winant[3], Myrl Hendershott[3], and Thomas Hayward[4]

[1]Atmospheric & Oceanic Science Program, Princeton University, Princeton, NJ 08544
(609) 258-5971, E-mail: lyo@splash.princeton.edu
[2]State University of New York, Stoney Brook, NY 11794
[3]Center for Coastal Studies, Scripps Institution of Oceanography, La Jolla, CA 92093-0209
[4]Marine Life Research Group, Scripps Institution of Oceanography, La Jolla, CA 92093

ABSTRACT

Previous works suggest that both wind and pressure gradient play important roles in determining the near-surface circulation in the Santa Barbara Channel (SBC). The results from a hindcast and nowcast model of currents in SBC for the recent El Niño winter and spring, from December 1997 through April 1998, were analyzed to infer the momentum balance in the channel. Two main forcing into the model were wind stresses and California Cooperative Oceanic Fisheries Investigations (CalCOFI) temperature and salinity (T/S) fields. Wind stresses were calculated by combining hourly National Data Buoy Center (NDBC) wind in the vicinity of the channel with historical, monthly COADS wind over the outer region away from the channel. Historical T/S fields were used to initialize the model, and together with CalCOFI data from December 1997 through April 1998, were assimilated into the modeled T/S by a simple nudging scheme. The assimilation of CalCOFI data introduced warmer water in the Southern California Bight (SCB).

The cross-channel balance was approximately geostrophic. The along-channel balance was primarily between wind, which was equatorward, sea-level tilt, which was poleward, and Coriolis, which was poleward if the wind was uniformly intense west and east of the channel, and was equatorward if the wind was much weaker in the east. The former wind condition induced southward cross-channel flow and would correspond to the observed 'Flood East' or 'Upwelling' scenario, while the latter northward cross-channel flow and to the 'Cyclonic' or 'Relaxation' scenario.

Keywords: Southern California Bight, eastern boundary currents, model nowcast, pressure gradients, wind curl.

INTRODUCTION

Located at the confluent region between the warm water of Southern California Bight (SCB) origin and the cooler upwelled water off the central California coast, and being partially sheltered from wind by the mountain range to its north, circulation in the Santa Barbara Channel (SBC; Figure 1) is driven by a combination of wind, windcurl, and thermal contrast. The equatorward wind in the SBC/SCB drives coastal currents near the surface which generally flow

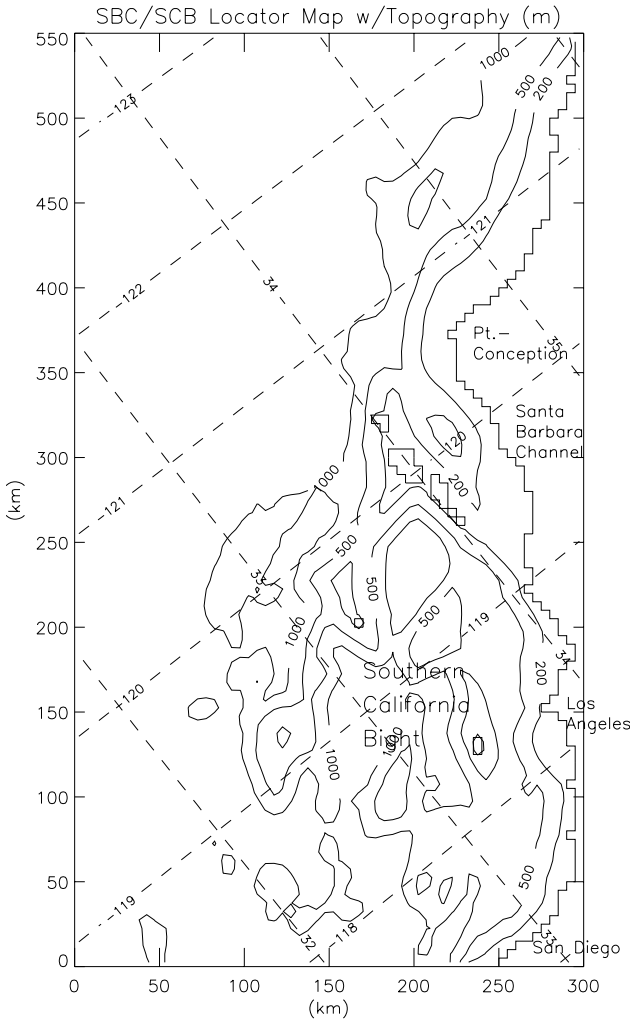

Figure 1. Santa Barbara Channel (SBC) and Southern California Bight (SCB) locator map and the model domain and topography. For computational efficiency, the deepest model's depth has been set to 2000m.

equatorward (e.g., Allen 1980). This holds true also in the SCB/SBC except that the situation is complicated by the intense windcurl at Point Conception that diminishes equatorward along the channel and the SCB coast. The equatorward weakening of the windcurl, which on the seasonal time scale peaks in summer, generates alongshore

pressure gradient, and drives poleward coastal flow (Oey 1996). Thus nearshore flows in the SCB/SBC can be envsioned as being driven by these two competing (and inseparable) mechanisms. The theory was originally intended to apply to seasonal time scales, but a more careful scaling analysis suggests that it should also be applicable to shorter time (O(10 days)) and smaller spatial (channel) scales (Oey 1999).

While the above idea can explain the origin of the alongshore pressure gradients, it does not directly address how the imbalances of these and the wind drive the channel's circulation. A tour de force analysis by Harms and Winant (1998) of 1994/1995 observations shows that near-surface currents in the channel are indeed a function of both wind and pressure gradient. One objective of the present paper is to understand the interplay between these two forcing components, and to reconcile theoretical ideas with those inferred from observations.

Our analyses are based on an application of the Oey's (1996) SBC/SCB model forced by realistic wind and thermal forcing. The model produces hindcast and nowcast of currents and temperature and salinity (T/S) fields during recent El Niño conditions from December 1997 through April 1998, when waters which were warmer than during normal conditions were found off the southern and central California coasts. The choice of a model with realistic bathymetry and forced by realistic wind and T/S fields, as opposed to a model with idealized settings, offers the advantage that inferences that are specific to the SBC/SCB system can be made. The down side is that the analysis will be more complex and simplifications will be necessary. The El Niño conditions also offer the opportunity of examining effects of heating (warm waters) from the south. The present results can also be used by: (1) the Office of Naval Research (ONR) in support of their field exercises in the channel, and (2) the Minerals Management Service (MMS) as basis for their surface flow trajectory analysis and Oil Spill Risk Analysis (OSRA).

THE MODEL

The model solves the finite-difference analog of the three-dimensional primitive equations assuming that the ocean is incompressible and hydrostatic, and using the Boussinesq approximation (details in Oey and Chen 1992). The model boundary conditions, domain and topography are the same as those used in Oey (1996; Figure 1), with two exceptions. The present application employs the coarse-grid only (i.e., the nested-grid option is turned off), with grid sizes $\Delta x = \Delta y = 5$ km and 30 equally-spaced sigma layers in the vertical. Secondly, a 200 km-wide sponge layer, within which the horizontal viscosity is linearly increased to ten times its interior value, is placed along the western open boundary. In combination with a radiation condition, the sponge damped westward-propagating Rossby waves and helped to prevent the development of a western boundary current.

Initial Condition and T/S Assimilation

Integration begins on December 16, 1997 and ends on May 5, 1998. The initial T/S fields were obtained from monthly climatological data set for December. These historical T/S were also used as boundary conditions during the integration. To account for the actual T/S conditions in 1997-1998, CalCOFI data from December 1997 and February-March 1998 cruises were assimilated into the model. While there were a number of cruise tracks, Line 90 (which spans offshore from the coast between Los Angeles and San Diego; Figure 2) only was used. The rationale is that T/S forcing from this southern location would propagate north to influence circulation in the channel. If CalCOFI T/S in and/or near the channel are also assimilated, questions related to incompatibility of data in the channel must also be addressed as the model attempts to adjust both to local and remote forcing.

The assimilation was accomplished as follows. The CalCOFI data at each standard level were first interpolated (extrapolated) onto the model grid using:

$$T_{ci} = \Sigma\, T_{cn} E_{ni} / \Sigma\, E_{ni} \tag{1a}$$

$$E_{ni} = \exp\{-\left[\left(x_{cn} - x_i\right)/ x_s\right]^2 - \left[\left(y_{cn} - y_i\right)/ y_s\right]^2\} \tag{1b}$$

where the summation Σ is over the total number 'N' of CalCOFI data points (i.e., n=1,N), T_{ci} denotes the interpolated value at the model's ith-grid point (x_i,y_i) (in degrees longitude and latitude, say), T_{cn} the nth-station CalCOFI value at (x_{cn},y_{cn}), and x_s and y_s are parameters that dictate the radius of influence of the CalCOFI data on the neighboring model grid points. Here, we take $x_s=y_s=0.25^o$.

Assimilated fields, T_{ai}, are next constructed using a weighted combination of the interpolated CalCOFI values, T_{ci}, and historical values, T_{hi}:

$$T_{ai} = W_i T_{ci} + \left(1 - W_i\right) T_{hi} \tag{2a}$$

$$W_i = \exp\left[-\min_n\left(R_{ni}\right)\right] \cdot \exp\{\left(Z_i / 200\right) - H_v\left(t - t_0\right).\left(t - t_0 / 30\right)\} \tag{2b}$$

$$R_{ni} = \left[\left(x_{cn} - x_i\right)/ x_s\right]^2 + \left[\left(y_{cn} - y_i\right)/ y_s\right]^2 \tag{2c}$$

where the minimum function 'min' checks over the total number 'N' of CalCOFI data points, z_i the vertical coordinate (=0 at surface and -H(x,y), where H=water depth, at the ocean bottom) in meters, t is time in days, t_o is time that

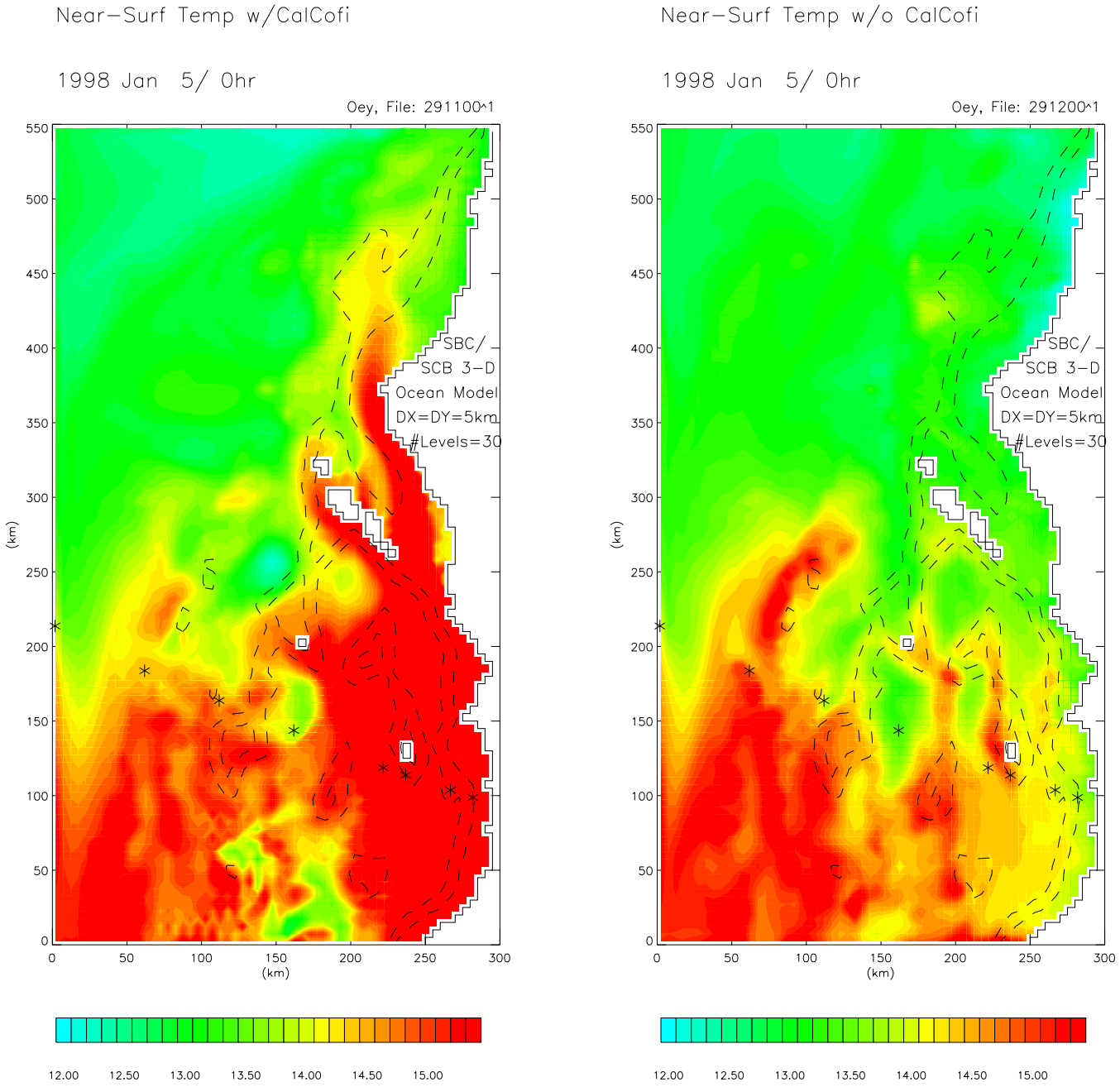

Figure 2. A comparison of the temperature fields at the first near-surface sigma level on January 5, 1998, with (left panel) and without (right panel) assimilation of the CalCOFI T/S along Line 90 (the starred points).

corresponds to April 15, 1998, and H_v is the Heaviside function. The spatial distribution of the weighting function, W_i, is such that, near the surface, it is ≈ 1 for model grid points near any of the CalCOFI stations, but decays exponentially away, and also with depth. Thus the assimilated field, T_{ai}, assumes CalCOFI for grid points near the cruise stations, and merges smoothly to historical field for points far away.

Finally, the assimilated field is inserted into the T/S transport equations as sources (i.e., the model was used in a so called 'robust diagnostic mode'):

$$\partial T / \partial t = \hat{e} + C \cdot (T_a - T) \qquad (3a)$$

$$C = W_i|_{z=0} \cdot \{G_d + (G_s - G_d) \cdot \exp(z/500)\} \qquad (3b)$$

where G_s=1/5 day^{-1} and G_d=1/300 day^{-1}, and similarly for the salinity, S. Thus for grid points near CalCOFI, the

modeled T/S are nudged back to CalCOFI with time scales of five days near the surface and 300 days in deeper layers. Away from CalCOFI stations, the T/S are nudged towards the historical T/S (because of Equation 2) but at increasing time scales (because of $W_i|_{z=0}$ in Equation 3) the calculation becomes essentially prognostic for distances > 50 km to 100 km away. In Figure 2, we compare the near-surface temperature fields on January 5, 1998 for runs with and without the CalCOFI nudging. It shows that, because of El Niño influence, the temperature with CalCOFI nudging is 1 to 2°C higher than 'climatology' especially near the coast where it is dynamically important. By this time (20 days into the integration), the warmer water has intruded into the channel and past Point Conception.

The Wind

The wind was specified by merging the hourly wind vectors (U_w) at NDBC stations in the vicinity of the channel (see Figure 3 for station sites) with climatological winds from COADS that cover the entire model domain (and beyond), as follows. The NDBC winds were first converted to wind stresses:

$$\tau_o = C_d \left| U_w \right| U_w \qquad \left(m^2 . s^{-2} \right) \tag{4}$$

where $C_d = 1.44 \times 10^{-6}$ for $|U_w| < 11$ m.s^{-1}, and = (0.49 + 0.065 $|U_w|$) $\times 10^{-6}$ otherwise. These were interpolated onto the model grid points using (1) with x_s=y_s=1.5°, and merged with COADS wind using equation (2a) (i.e., with NDBC replacing T_{ci} and COADS replacing T_{hi}). However, the weighting function is simpler = E_{ni}, where the (x_{cn},y_{cn}) in (1b) is taken as fixed equal to (-120°12', 34°24'), the center of gravity of the NDBC sites used. For the simulation period, data were available at seven sites in the vicinity of the channel (those marked '⊕' in Figure 3), but was missing at station 46053 (marked '+'). Data from previous years (e.g., Harms and Winant 1998) indicates that wind at this site is weak and more similar to stations to the east and south than to stations in the western mouth of the channel. The wind at station 46053 is therefore equated to that at station 46045. Figure 3 shows an example of the result of the NDBC/COADS wind merging at two times, winter and spring. An important aspect is wind weakening from west to east of the channel, and also to the south over the Southern California Bight.

RESULTS

We first present results for the experiment (Experiment A; Table 1) in which the wind and T/S are prescribed as in previous section. However, to gain further insights, other experiments with different wind and T/S forcing have also been conducted. Figure 4 shows daily averaged surface temperature, elevation (η) and currents (u,v) at surface and at 100 m depth on March 16 and April 15, 1998. The two dates are chosen to illustrate two different dynamical regimes as wind (March 16) and windcurl (April 15) forcing compete in driving near-coast flows in region southeast of SBC (Oey 1996,1999). In Figure 4a, flow in this region is equatorward caused by upwelling favorable wind that began to strengthen near the beginning of March. A cyclone also begins to form at the western portion of the channel. This we will see depends critically on the relative strength of the wind at NDBC stations 46054 and 46053. Cooler water, as well as a dip in free-surface elevation, can be seen at the cyclone center. By April, poleward flow is seen southeast of SBC. Its appearence can be explained in terms of equatorward weakening of windcurl along the coast in the SCB, and the subsequence set-up of an along-coast pressure gradient (compare the elevation contours in Figures 4a,b; Oey 1996,1999).

Momentum Balance

To elucidate the dynamics, we resolved the model velocities in the near-coast region into cross-isobath (*x* and u; positive shoreward) and along-isobath (*y* and *v*; positive poleward) components. We find that the cross-isobath momentum balance is to a good approximation geostrophic. The along-isobath momentum equation is:

$$\underset{\text{I}}{dv/dt} + \underset{\text{II}}{fu} + \underset{\text{III}}{g \cdot \partial\eta/\partial y} - \underset{\text{IV}}{\partial\left(K . \partial v/\partial z\right)/\partial z} + \underset{\text{V}}{\left(g/\rho_o\right) . \int_z^0 \partial\rho/\partial y \, . \, \partial z' = 0} \tag{5}$$

where $d/dt = \partial/\partial t + \mathbf{u} . \nabla$, K the eddy viscosity coefficient (m^2/s), ρ the density (kg/m^3), g = 9.8 m/s^2, f the Coriolis parameter (s^{-1}), and a small term arising from the curvature of the isobath (coastline) is omitted. Each term in Equation 5 was calculated beginning with the 50 m isobath near the coast, and to 40 km offshore, and averaged cross-isobath and also in time (note that in the SBC, this averaging encompasses the entire channel width). We find that term I, and also term V for the near-surface grid layer, are small. Figure 5 shows the three remaining terms for the near-surface grid as a function of the alongshore distance. Plotted is also the term that represents friction acting at the base of the near-surface layer; i.e., the term IVb on the right hand side of

$$\underset{\text{IVa}}{\partial\left(K . \partial v/\partial z\right)/\partial z \approx \tau_o^y / \Delta z} - \underset{\text{IVb}}{\left(K . \partial v/\partial z\right)\big|_{base} / \Delta z} \tag{6}$$

where τ_o^y is the along-isobath wind stress and Δz (15m) is the thickness of the layer. Figure 5 shows that this friction term is small, and wind stress therefore dominates the shear term IV, which is negative along the entire coast (i.e., equatorward; note that the negative of term IV is plotted). Thus, to a good

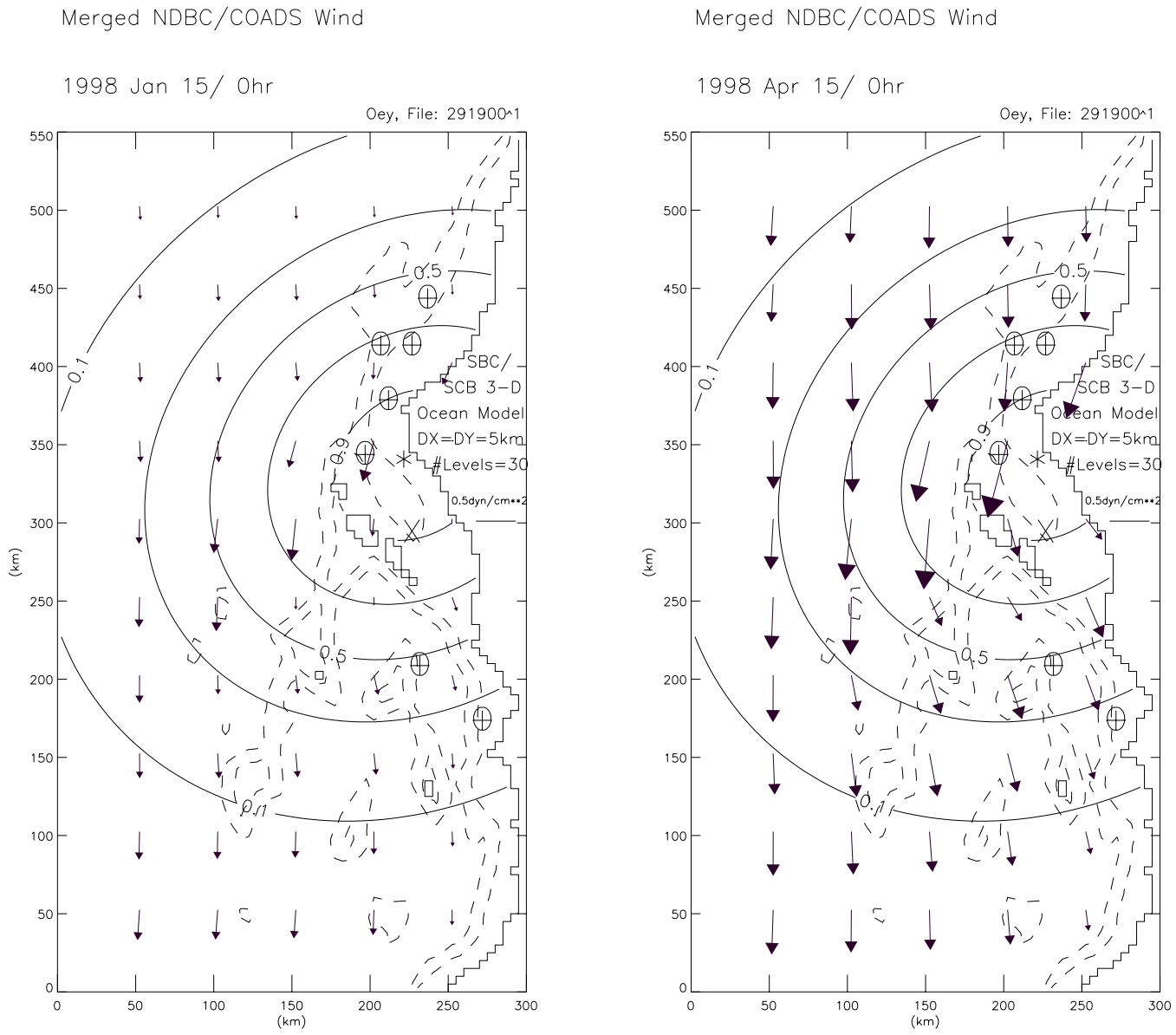

Figure 3. The 10-day averaged wind vectors on January 15 and April 15, 1998. Locations of national Data Buoy Center (NDCB) wind stations used in the simulation are marked as '⊕'. They are, from northwest to southeast: 46062, 46011, 46023 (offshore) and 46045. An additional station, marked as 'x' (NDBC station 46053) was also used (see text). The location of center of gravity of these stations is marked as '*'. The contours give the weighting function used to merge the NDBC with COADS winds (see text).

Table 1. Model experiments.

Experiment	Winds COADS	Winds NDBC	T/S Assimilation Historical	T/S Assimilation CalCOFI	Wind Merging Scales X_s & Y_s	NDBC Buoy # 46053 Set to:
A	*	*	*	*	1.5	46045
B	*	*	*	*	1.5	-
C	*	*	*	-	1.5	46045
D	*	*	*	-	1.5	-
E	*	*	*	*	3	46045
F	*	*	*	*	1.5	46025

A star '*' or number means that the item was applied in the model.
A dash '-' means that the item was omitted.

approximation, the alongshore balance is between the equatorward wind and the pressure gradient (III) and Coriolis (II) terms. We note also that the friction term IVb is positive, which means that the alongshore currents near the surface, being wind-driven, are more equatorward than currents in the lower layer. This is generally true also for all other experiments to be discussed below, and the frictional force is poleward opposing the wind.

Balance in the Southern California Bight

From San Diego (SD) to about 100 km north, sea level slopes upward (i.e., III is positive). This is because off 33.5°N ($y \approx 100$ km) the equatorward wind, hence its curl, is weakest, and also warmer water is being assimilated from

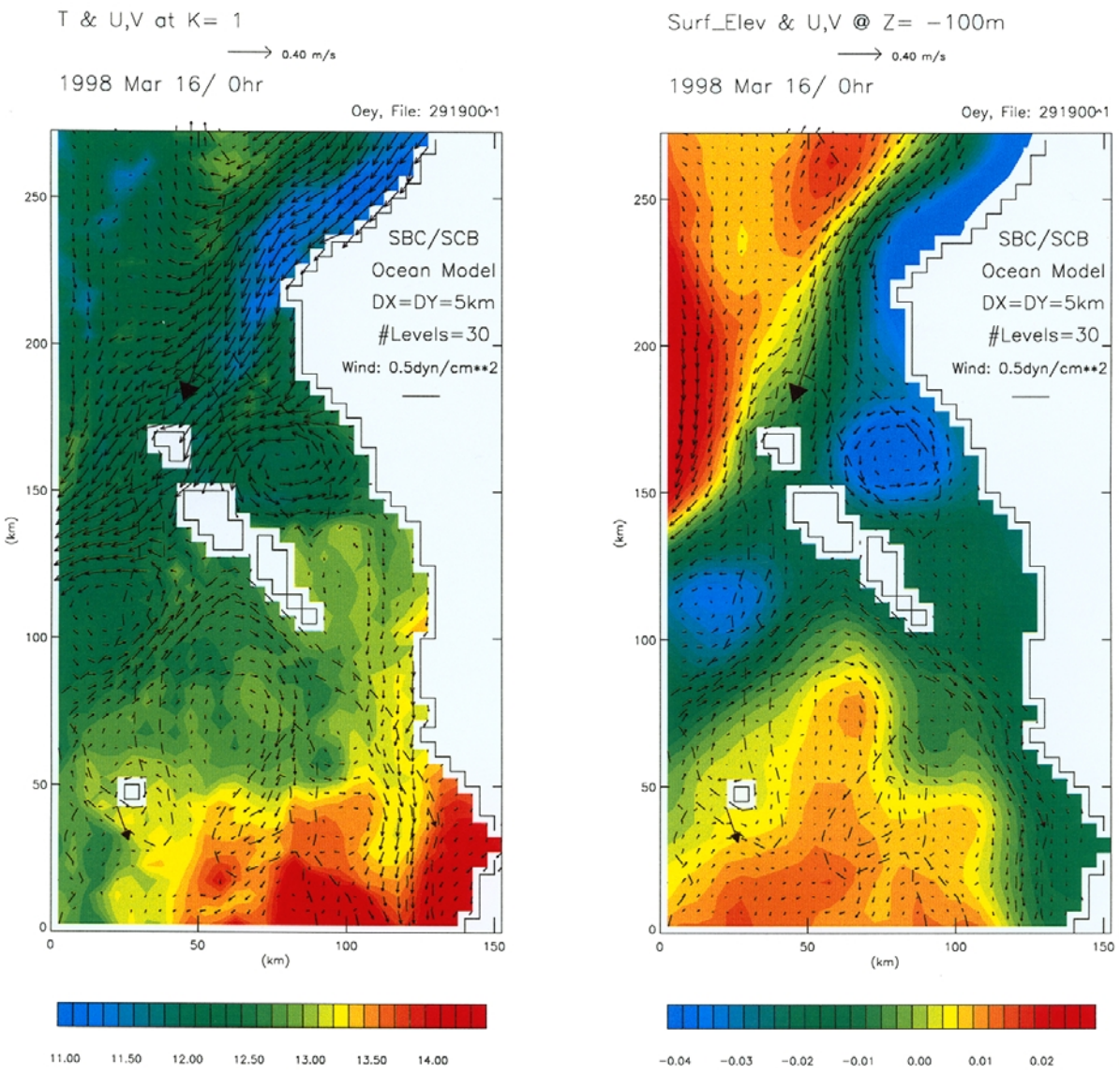

Figure 4A. The one-day averaged temperature (°C) and currents at the first model grid point near the surface (left panel), and elevation (m) with currents at z=-100m (right panel), for (a) March 16 and (b) April 15, 1998, in a blow-up region that focuses on the Santa Barbara Channel and vicinity. Five-day averaged wind stresses are also plotted as vectors with thick arrows at four locations.

CalCOFI stations. Both mechanisms interact because of density advection, but in general induce a local high. That wind weakens off 33.5°N is supported by the extensive analysis of data from buoys and ship observations by Winant and Dorman (1997), but the second mechanism is a model artifact caused by assimilation (in reality, warmer El Niño water extends from the south). The positive sea-level gradient and equatorward wind stress are balanced, geostrophically and through Ekman dynamics, by the negative Coriolis term II caused by offshore flow south of the anticyclonic high.

Further north, the pressure gradient switches to negative as sea level tilts downward by about 3 cm over the 200 km alongshore distance from Los Angeles (LA) to Point Conception (PC). Just north of LA, pressure gradient is balanced by equatorward wind stress and the acceleration caused by onshore flow (term II is positive) on the north side of the coastal anticyclone. Further north and into the eastern SBC (y ≈ 260 km), offshore flow develops consistent with wind-driven Ekman dynamics, the resulting poleward acceleration combines with pressure gradient to balance the equatorward wind stress.

Balance in the Santa Barbara Channel

From eastern SBC to the central channel (y ≈ 300 km), wind stress and hence its offshore (i.e., from north to south across the channel) Ekman flux remain approximately

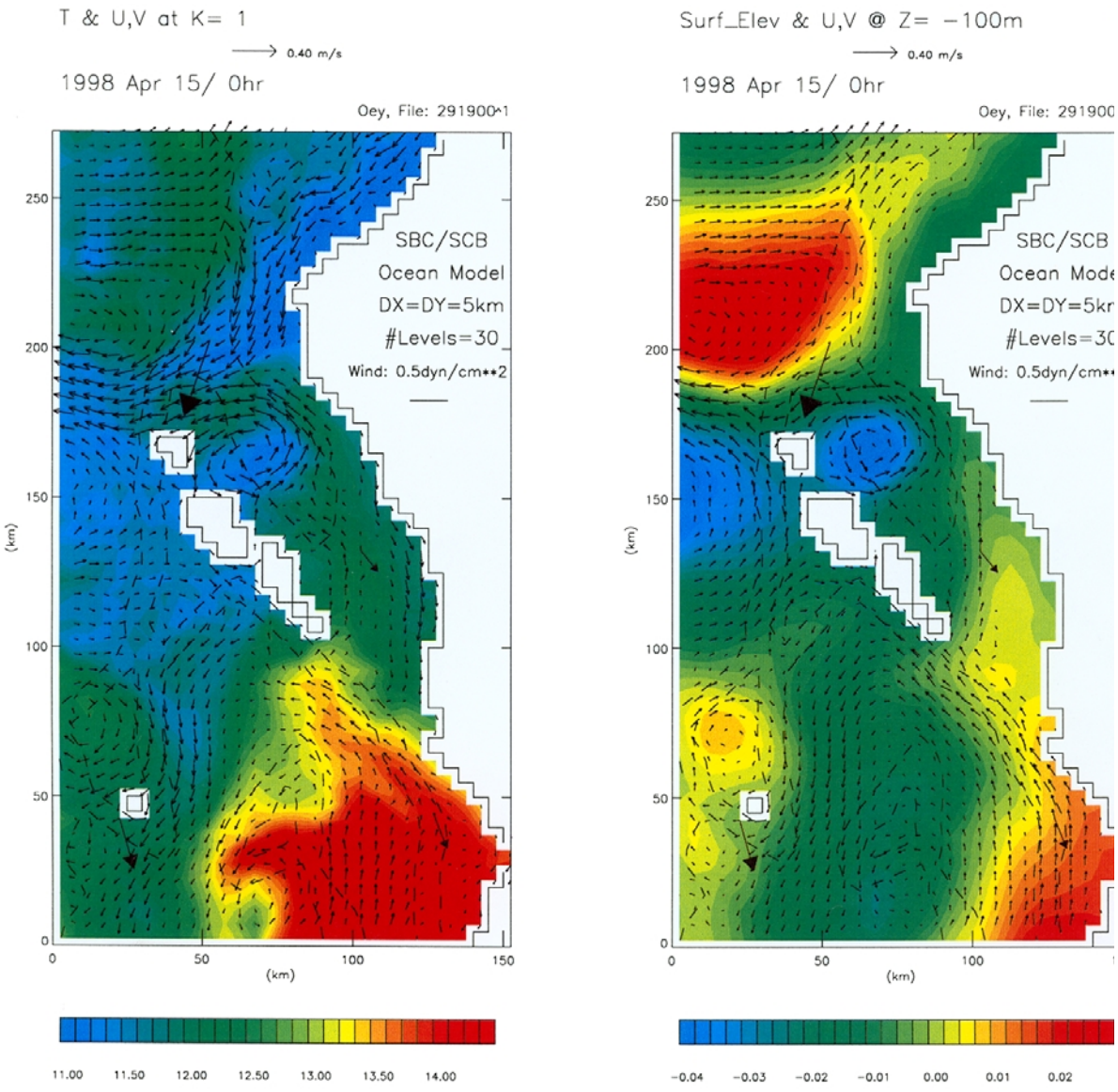

Figure 4B. The one-day averaged temperature (°C) and currents at the first model grid point near the surface (left panel), and elevation (m) with currents at z=-100 m (right panel), for April 15, 1998, in a blow-up region that focuses on the Santa Barbara Channel and vicinity. Five-day averaged wind stresses are also plotted as vectors with thick arrows at four locations.

equal to their values to the south (recall that for Experiment A, wind at 46053 = 46045), but downward tilt of sea level increases towards the cyclone low in the western channel. The excess pressure gradient forces an onshore flux that reverses the wind-driven Ekman component at the mid-channel (280 km < y < 310 km). This mechanism depends crucially on differential wind strength west and east of the channel. Figure 6 shows the balance plot for Experiment B, for which wind at 46053 was not explicitly specified, and was therefore, essentially extrapolated from the western channel station 46054 using (1) as described previously. The wind in the eastern portion of the channel is therefore similar to that in the west, and is intense during the spring transition period beginning in March. Comparing Figure 6 with Figure 5, differences in the balance can be seen from y = 220 km (southeast of the SBC) to PC. For Experiment B, (the negative of) shear term IV (due to wind) begins to increase near y = 220 km, instead of near y = 300 km (mid-channel) for Experiment A (Figure 5). The result is that offshore (southward) Ekman flux persists in the eastern channel for Experiment B. Also, the friction term (IVb) is larger, caused by more intense mixing by strong wind in the channel, although the shear term IV is still dominated by the wind stress term IVa. Thus the summed poleward acceleration caused by the Coriolis of this Ekman flux, sea-level tilt, and friction, is balanced by the equatorward acceleration due to wind.

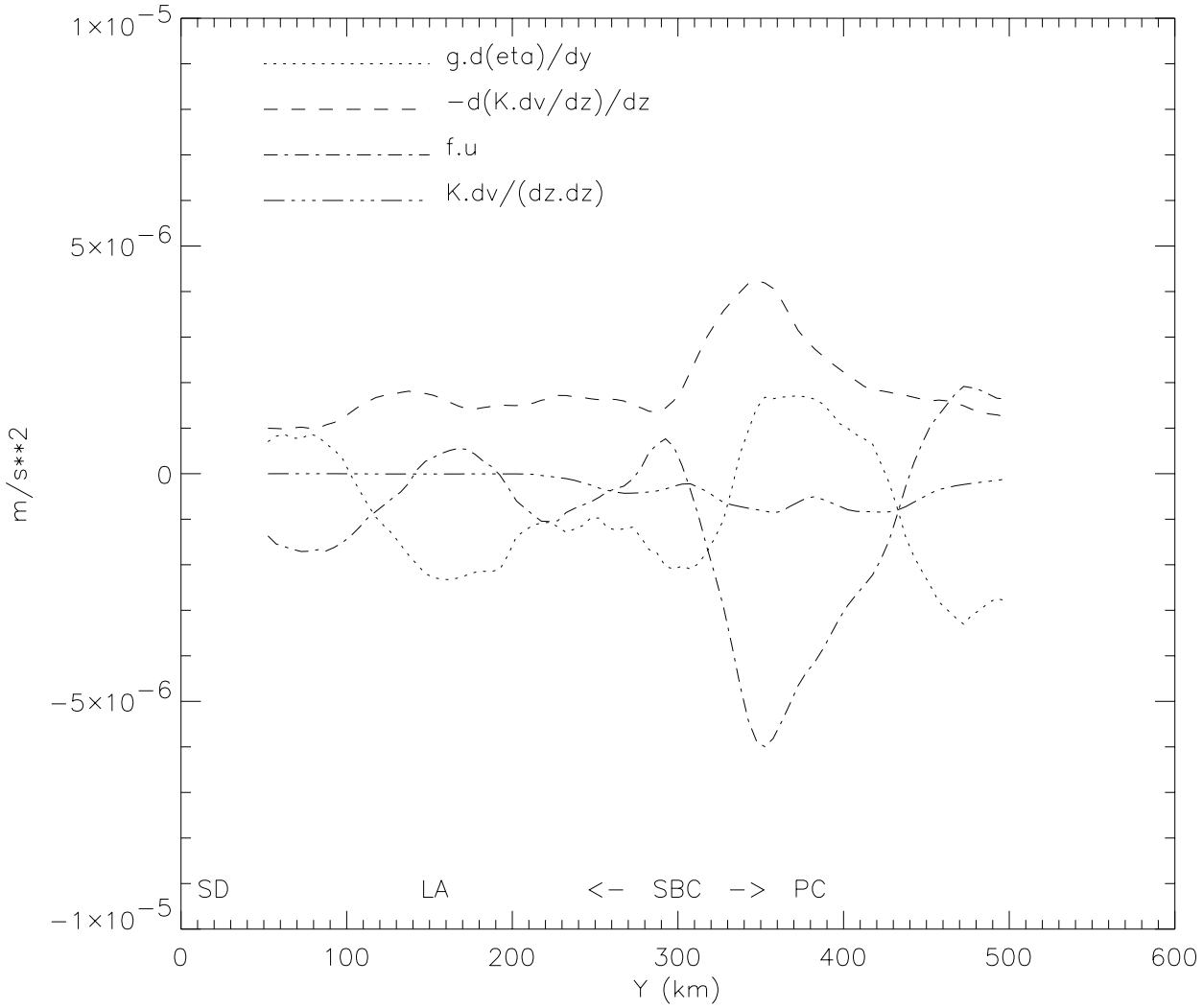

Figure 5. The three dominant terms: pressure gradient (dotted), vertical shear (dashed) and Coriolis (dash-dot), and the term that represents friction at the base of the layer (dash with 3 dots), in the along-isobath momentum balance in the model's near-surface layer for Experiment A. Geographical locations along Y are, SD: San Diego, LA: Los Angeles, SBC: Santa Barbara Channel, and PC: Point Conception.

In summary (Figure 7), the near-surface flow in SBC can be viewed as being due to an imbalance between poleward (westward) sea-level tilt and equatorward (eastward) wind stress. An excess of the former, caused by weakened wind in the eastern portion of the channel, generally leads to a south-to-north cross-channel flow that helps to reinforce the cyclonic re-circulation in the west, as well as the likelihood that poleward flow develops in the channel (State I). The reverse (State II) leads to a north-to-south cross-channel Ekman flux near the surface, and the situation is more akin to classical upwelling problems, which in general would result in equatorward flow in the channel. We have shown that the establishment of one state versus the other depends crucially on the relative magnitude of the wind stresses west and east of the channel.

The momentum balance gives no clue as to how the western cyclone is formed; i.e., if the cyclone is a result of successions of State I caused originally by equatorward weakening of the windcurl, or is locally spun up (by windcurl or flow separation). It is clear that, however it is produced, the cyclone dynamically contributes to the sea-level tilt.

Balance at Point Conception and North

Near and to the north of Point Conception, the sea-level gradient term III changes sign to become positive, induced by the cyclone low at the western SBC. The resulting equatorward acceleration reinforces that from the intense wind stress along the central California coast. Given that friction and other terms in the alongshore balance are small, these must be balanced by a poleward acceleration due to the Coriolis term. Thus the coastal jet acquires an offshore component that is most intense just south of Point Conception where both the wind and upward sloping of the sea-level are maximum (Figure 5), and the jet has a tendency to veer offshore (Figure 4).

North of y ≈ 420 km, sea-level tilts downward. This is a model artifact due to northward advection of warmer water from the south. A warm eddy was present off y ≈450 km

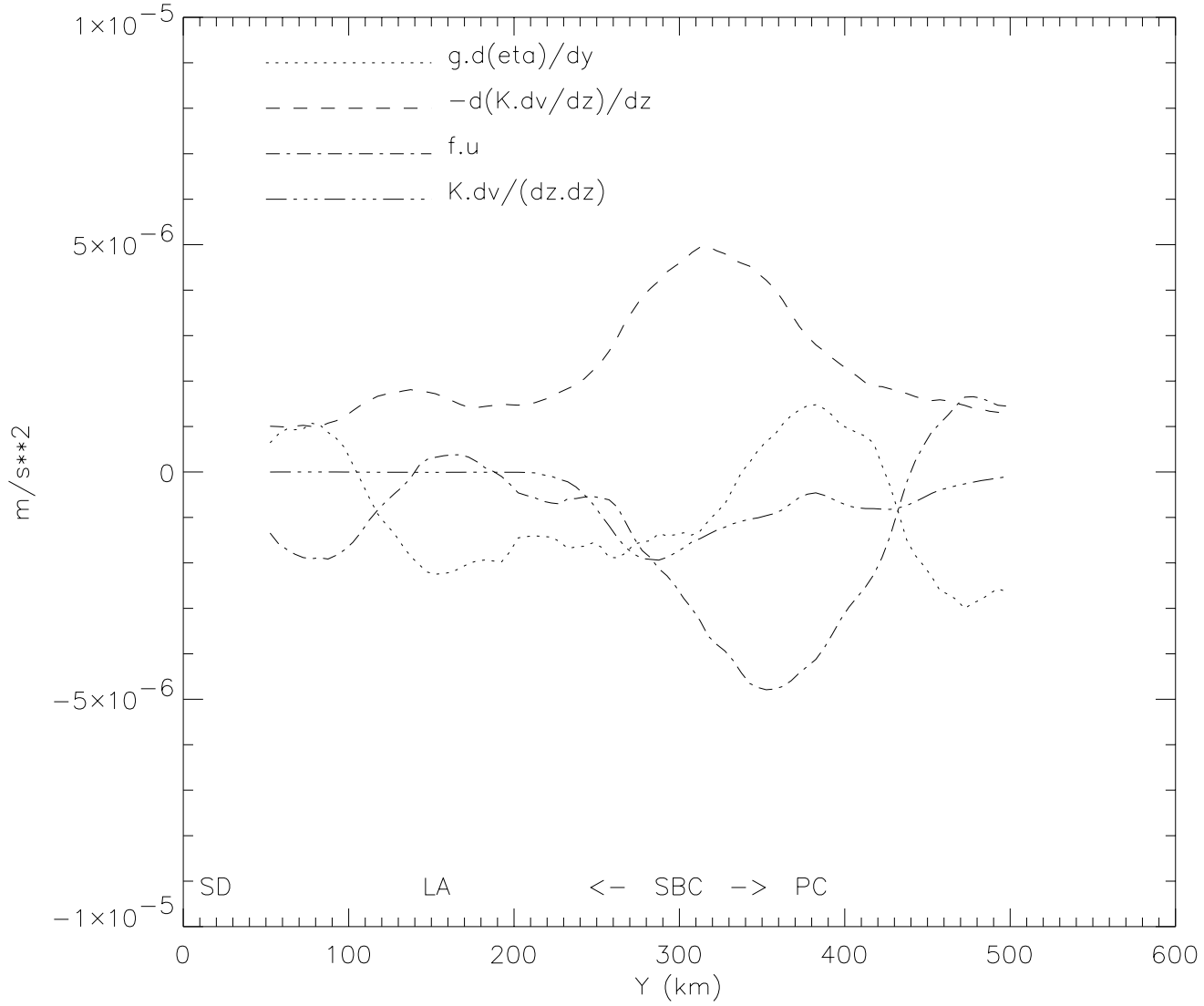

Figure 6. The three dominant terms: pressure fgradient (dotted), vertical shear (dashed) and Coriolis (dash-dot), and the term that represents friction at the base of the layer (dash with 3 dots), in the along-isobath momentum balance in the model's near-surface layer for Experiment B. Geographical locations along Y are, SD: San Diego, LA: Los Angeles, SBC: Santa Barbara Channel, and PC: Point Conception.

after about 20 to 30 days of simulation (c.f. Figure 2, left panel), and slowly dispersed westward. To its north, the eddy produced onshore flow and downward tilt of sea-level.

Balance in Other Experiments

When CalCOFI T/S was not assimilated (Experiment C or D), the strong poleward flow in December 1997 and January 1998 for Experiments A and B was now absent. However, because of upwelling in March and April, warmer water in Experiments A and B was confined to the southern region (the SCB), and the dynamic balance in the channel was similar with or without CalCOFI T/S. It is likely that, had the integration been extended to cover summer and fall, the effects of warmer water would be more apparent.

Finally, the model results also changed little when the values of x_s and y_s in the weighting function used to merge the NDBC with COADS winds were changed from 1.5° to 3° (Experiment E). The results are also not sensitive to which of the two NDBC wind data in the southeastern-most stations (46045 – Experiment A or 46025 –Experiment F) was used for the missing wind station NDBC 46053.

DISCUSSION AND CONCLUSIONS

Three dominant terms in the alongshore momentum balance of the coastal circulation in the SBC/SCB from December 1997 through April 1998 are wind, which is equatorward, pressure gradient, which is poleward, and Coriolis due to cross-shore flows, which can be poleward or equatorward. In the SBC, we have identified two distinct states of circulation that depend critically on the distribution of wind stress in the channel. For winds with approximately equal strengths west and east of the channel, the along-channel component produces southward Ekman flow

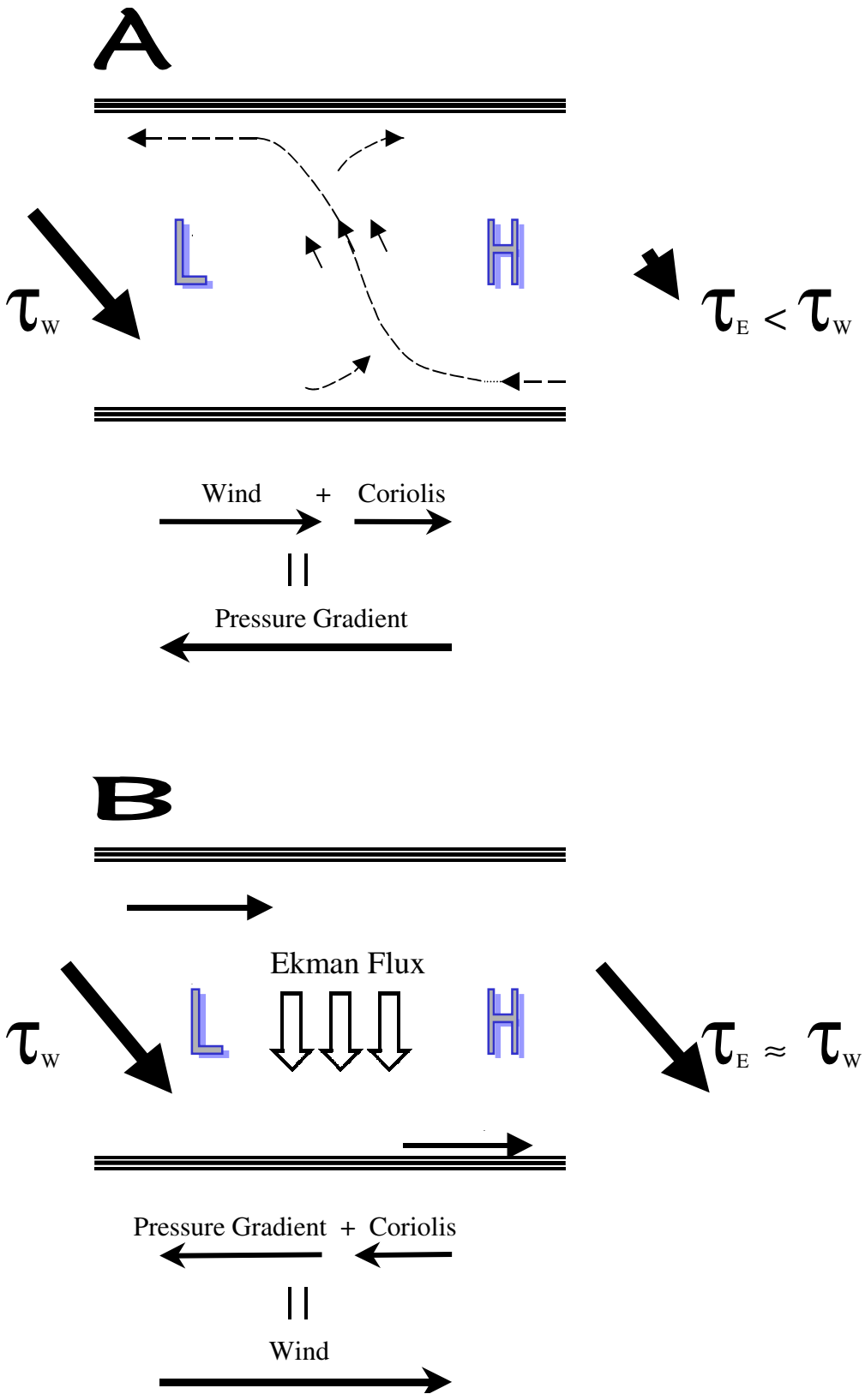

Figure 7. **A schematic summary of flow balance in the Santa Barbara Channel for (a) Experiment A: wind in east is weaker than that in west, and (b) Experiment B: wind in east is of the same magnitude as that in west.**

across the channel that together with the pressure gradient balances the wind. The along-channel flow then tends to be uniformly equatorward with no cyclonic recirculation in the west. This (State II) would correspond to either the Upwelling or Flood East characteristic patterns described in Harms and Winant (1998). We may expect that the same requirement of uniformity in wind, but reversed in direction, would lead to the Flood West pattern. On the other hand, for wind that is intense in the west but weak in the east, the wind-induced Ekman flow is overcome by the south-to-north cross-channel flow generated by the pressure gradient. This cross-channel flow occurs near and to the east of the mid-channel where wind stress is weak. This (State I) would tend to produce a cyclonic recirculation in the west and would correspond to either the Cyclonic or Relaxation characteristic patterns described in Harms and Winant (1998). In both states, the cross-channel flow serves as an important index that characterizes the imbalance between wind and pressure gradient.

A comparison of the pressure gradient terms in Figures 5 and 6 show that they are of comparable magnitudes, although in the non-uniform wind case (Figure 5), the presence of a cyclone in the west induced a larger sea-level tilt. This suggests that a large portion of the sea-level gradient is caused by larger scale windcurl and heating over the SCB. One also ponders upon the chicken-and-egg question of whether the cyclone is formed by an aggregate of State-I events, or is purely local induced by localized windcurl and flow separation, say, and hence helps to promote the State-I event. This clearly requires further research.

Finally, the types of dynamic balance described here are of significant practical value. They help to identify forcing patterns that may then be used as key predictive parameters in future hindcast/nowcast studies.

ACKNOWLEDGMENTS

This work was funded by the Office of Naval Research (LYO) and the Minerals Management Service (MMS). Computing was performed at the Geophysical Fluid Dynamic Laboratory, Princeton, and the San Diego Supercomputer Center.

LITERATURE CITED

Allen, J. S. 1980. Models of wind-driven currents on the continental shelf. Annual Review of Fluid Mechnics 12:389-433.

Harms, S. and Winant, C. D. 1998. Characteristic patterns of the circulation in the Santa Barbara Channel. Journal of Geophysical Research 103:3041-3065.

Oey, L.-Y. and P. Chen. 1992. A nested-grid model simulation of the Norwegian coastal current. Journal of Geophysical Research 97:20,063-20,086.

Oey, L.-Y. 1996. Flow around a coastal bend: a model of the Santa Barbara Channel eddy. Journal of Geophysical Research 101:16,667-16,682.

Oey, L.-Y. 1999. A Forcing Mechanism for the Poleward Flow off the Southern California Coast. Journal of Geophysical Research, 104:13,529-13,539.

Winant, C. D. and C. E. Dorman. 1997. Seasonal patterns of surface wind stress and heat flux over the Southern California Bight. Journal of Geophysical Research 102:5,641.